DOI: 10.1002/chem.200601786

Three-Dimensional Lanthanide(III)–Copper(II) Compounds Based on an Unsymmetrical 2-Pyridylphosphonate Ligand: An Experimental and Theoretical Study

Yun-Sheng Ma,[a] Hui Li,[b] Jun-Jie Wang,[a] Song-Song Bao,[a] Rong Cao,[c] Yi-Zhi Li,[a] Jing Ma,*[b] and Li-Min Zheng*[a]

Abstract: Based on an unsymmetrical 2-pyridylphosphonate ligand, two types of Ln^{III}–Cu^{II} compounds with three-dimensional structures were obtained under hydrothermal conditions, namely, $Ln_2Cu_3(C_5H_4NPO_3)_6{\cdot}4H_2O$ (**1·Ln**; Ln = La, Ce, Pr, Nd) and $Ln_2Cu_3(C_5H_4NPO_3)_6$ (**2·Ln**; Ln = Pr, Nd, Sm, Eu, Gd, Tb, Dy, Ho). Compounds **1·Ln** are isostructural and crystallize in chiral cubic space group $I2_13$. In these structures, each Ln ion is nine-coordinate and has a tricapped triprismatic geometry, while each Cu center is six-coordinate with an octahedral environment. The $\{LnO_9\}$ polyhedra and $\{CuN_2O_4\}$ octahedra are connected by edge sharing to form an inorganic open framework structure with a 3-connected 10-gon (10,3) topology in which the Ln and Cu atoms are alternately linked by the phosphonate oxygen atoms. Compounds **2·Ln** are isostructural and crystallize in trigonal space group $R\bar{3}$. In these structures, the $\{LnO_6\}$ octahedra are triply bridged by the $\{CPO_3\}$ tetrahedra by corner sharing to form an infinite chain along the *c* axis. Each chain is connected to its six equivalents through corner sharing of $\{CPO_3\}$ tetrahedra and $\{CuN_2O_2\}$ planes to form a three-dimensional framework structure in which the Ln and Cu atoms are linked purely by O-P-O units. The formation of these two types of structures is rationalized by quantum chemical calculations, which showed that both the lanthanide contraction and the electron configuration of Cu^{II} play important roles. When Cu^{II} was replaced by Zn^{II}, only the first type of compounds resulted. The magnetic properties of complexes **1·Ln** and **2·Ln** were investigated. The nature of Ln^{III}–Cu^{II} (Ln = Ce, Pr, Nd) interactions is illustrated by comparison with their Ln^{III}–Zn^{II} analogues.

Keywords: copper · hydrothermal synthesis · lanthanides · magnetic properties · N,O ligands

Introduction

Lanthanide-containing paramagnetic systems are appealing for molecule-based magnets, particularly for designing single-molecule and single-chain magnets, due to the large anisotropy associated with most of the lanthanides.[1–4] Since the pioneering work of Gatteschi et al.,[5] a large number of heterometallic lanthanide(III)–copper(II) complexes have been described and their magnetic properties studied.[6–13] The majority of them, however, are restricted to the Gd^{III}–Cu^{II} system, because the Gd^{III} ion with f^7 electron configuration has an orbitally nondegenerate ground state. More interestingly, the Gd^{III}–Cu^{II} interaction is ferromagnetic, almost irrespective of the nature of the ligand.[1] Although a few exceptions are observed,[13,14] quantum-chemical calculations on a binuclear Gd^{III}–Cu^{II} complex reveal that the ferromagnetic gap between ground $S=4$ and the next $S=3$ state is intrinsic to the Gd^{III}–Cu^{II} systems within the C_{2v} sym-

[a] Y.-S. Ma, J.-J. Wang, S.-S. Bao, Prof. Y.-Z. Li, Prof. L.-M. Zheng
State Key Laboratory of Coordination Chemistry
Coordination Chemistry Institute
School of Chemistry and Chemical Engineering
Nanjing University, Nanjing 210093 (P. R. China)
Fax: (+86) 25-8331-4502
E-mail: lmzheng@netra.nju.edu.cn

[b] H. Li, Prof. J. Ma
Theoretical and Computational Chemistry Institute
School of Chemistry and Chemical Engineering
Nanjing University, Nanjing 210093 (P. R. China)
Fax: (+86) 25-8368-6467
E-mail: majing@nju.edu.cn

[c] R. Cao
State Key Laboratory of Structure Chemistry
Fujian Institute of Research on the Structure of Matter
The Chinese Academy of Sciences, Fuzhou 350002 (P. R. China)

Supporting information for this article is available on the WWW under http://www.chemeurj.org/ or from the author.

metry of the molecular prototype.[15] In the case of pronounced asymmetry, the usual configuration interaction forces related to kinetic transfer override the intrinsic ferromagnetic part, and this leads to antiferromagnetic exceptions.[15]

For the other lanthanide(III) ions, the presence of a first-order orbital momentum makes the understanding of the 4f–3d interactions more difficult. Each of the $^{2S+1}L_J$ states arising from the $4f^n$ configuration due to interelectronic repulsion and spin–orbital coupling will be further split into Stark components by the crystal-field perturbation. Hence, the temperature dependence of $\chi_M T$ is attributed to both thermal depopulation of the Ln^{III} Stark components and Ln^{III}–Cu^{II} couplings.[1,7] The approach proposed by Kahn et al. to understand the true nature of the Ln^{III}–Cu^{II} interactions is to compare the magnetic properties of isostructural Ln^{III}–Cu^{II} and Ln^{III}–Zn^{II} compounds. Following this approach, they concluded that the Tb^{III}–Cu^{II} and Dy^{III}–Cu^{II} interactions are also ferromagnetic, while the Ho^{III}–Cu^{II} interaction is not, which is not in line with the prediction that the Ln^{III}–Cu^{II} interaction is expected to be antiferromagnetic for Ln^{III} ions with fewer than seven 4f electrons and ferromagnetic otherwise.[7] To date, it is still a challenge to determine not only the magnitude but also the nature of the Ln^{III}–Cu^{II} interactions. More work is required to clarify these questions.

Here we show that two types of Ln^{III}–Cu^{II} compounds with three-dimensional structures can be obtained based on an unsymmetrical 2-pyridylphosphonate ligand, namely, $Ln_2Cu_3(C_5H_4NPO_3)_6{\cdot}4H_2O$ (**1·Ln**; Ln = La, Ce, Pr, Nd) and $Ln_2Cu_3(C_5H_4NPO_3)_6$ (**2·Ln**; Ln = Pr, Nd, Sm, Eu, Gd, Tb, Dy, Ho). To understand the nature of the Ln^{III}–Cu^{II} interactions in **1·Ln**, compounds $Ln_2Zn_3(C_5H_4NPO_3)_6{\cdot}4H_2O$ (**Ln_2Zn_3**; Ln = Ce, Pr, Nd), which are isostructural to **1·Ln**, were also prepared for comparison. To the best of our knowledge, these are the first examples of lanthanide–transition metal heterometallic phosphonates, even though a number of lanthanide phosphonate compounds have been reported so far.[16]

Results and Discussion

Syntheses: Complexes **1·Ln** were prepared as single phases by hydrothermal reactions of $Cu(O_2CCH_3)_2{\cdot}H_2O$, lanthanide(III) nitrate, and 2-pyridylphosphonic acid (2-$pyPO_3H_2$) in the molar ratio of 3:2:6 at 140 °C. When the molar ratio of these starting materials was changed to (1/2–1):(1/3–1):1, crystals of **1·Ln** were obtained together with uncharacterized pale precipitates. Complexes **1·La** and **1·Ce** can also be obtained as single phases by replacing $Cu(O_2CCH_3)_2{\cdot}H_2O$ by $Cu(NO_3)_2{\cdot}3H_2O$, $CuSO_4$, or $CuCl_2{\cdot}2H_2O$. When $CuSO_4$ was treated with $Pr(NO_3)_3{\cdot}6H_2O$ (or $Nd(NO_3)_3{\cdot}6H_2O$) and 2-$pyPO_3H_2$, pale blue, cubic crystals of complex **1·Pr** (or **1·Nd**) were obtained together with purple platelike crystals of **2·Pr** (or **2·Nd**). The latter can be manually selected from the mixture by judging the color and form of the crystals. Pure and large purple platelike crystals of the other **2·Ln** compounds (Ln = Sm, Eu, Gd, Tb, Dy, Ho) can only be prepared by using $CuSO_4$ as the copper source in reactions with lanthanide(III) nitrate and 2-$pyPO_3H_2$ in the molar ratio of 3:2:6. Replacement of $CuSO_4$ by the other copper salts results in only pale purple powder. Compounds **2·Ln** are not stable in the mother liquor and are completely transformed into $Cu(2\text{-}C_5H_4NPO_3H)_2$[17] when their crystals are kept in the mother liquid for a few days. For compounds **Ln_2Zn_3**, only the first type of compounds is obtained for all these lanthanide ions, no matter which kind of zinc source is employed.

Description of crystal structures

*$[Ln_2Cu_3(C_5H_4NPO_3)_6]{\cdot}4H_2O$ (**1·Ln**; Ln = La, Ce, Pr, Nd)*: Compounds **1·Ln** are isostructural and crystallize in cubic space group $I2_13$. Taking **1·La** as an example, the asymmetric unit consists of 1/3 La atoms, 1/2 Cu atoms, one 2-$pyPO_3^{2-}$ ligand, and two 1/3 H_2O molecules. Figure 1 shows

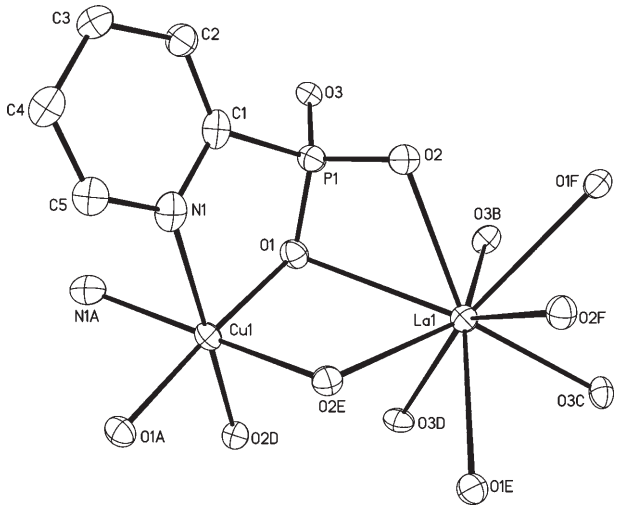

Figure 1. Building block of structure **1·La** with atomic labeling scheme (thermal ellipsoids at 30% probability). The symmetry codes are the same as those in Table 2.

the building block of **1·La** with atomic labeling scheme. The La1 atom is located at a threefold axis and has a tricapped triprismatic geometry. The nine coordination sites around La1 are occupied by phosphonate oxygen atoms (O1, O2, O1E, O1F, O2E, O2F, O3B, O3C, O3D) from six equivalent 2-$pyPO_3^{2-}$ ligands. The La1–O1 bond length of 2.778(6) Å is longer than the La1–O2 (2.545(5) Å) and La1–O3 (2.415(5) Å) distances. The Cu1 atom is located at a special position (0.5, 0.75, 0.266388) and has a distorted octahedral geometry. The six coordination positions are filled with four phosphonate oxygen atoms (O1, O1A, O2D, O2E) and two pyridyl nitrogen atoms (N1, N1A) from four equivalent 2-$pyPO_3^{2-}$ ligands. The Cu1–N1, Cu1–O1, and Cu1–O2D distances are 1.965(5), 2.180(8), and 2.137(5) Å, respectively.

Each 2-pyPO$_3^{2-}$ ion acts as a tetradentate chelating and bridging ligand. It chelates the La atom through phosphonate oxygen atoms O1 and O2, and the Cu atom through phosphonate oxygen atom O1 and pyridyl nitrogen atom N1. The remaining phosphonate oxygen atom O3 is coordinated to the other equivalent La atoms. Both O1 and O2 serve as μ_3-O bridges and link the Cu1 and La1 atoms in a LaO_2Cu four-membered ring with Cu1-O1-La1 and Cu1-O2E-La1 angles of 103.1(2) and 106.0(2)°, respectively. The dihedral angle between the Cu1O1O2E and La1O1O2E planes is 17.6°. The Cu1···La1 separation across the μ_3-O bridge of 3.748 Å is much shorter than the M···M separations across the O-P-O unit (Cu···La 6.584, La···La 5.762, Cu···Cu 5.953 Å). Consequently, each $\{CuN_2O_4\}$ octahedron shares edges with two $\{LaO_9\}$ tricapped triprisms, and each $\{LaO_9\}$ unit with three $\{CuN_2O_4\}$ octahedra. A three-dimensional inorganic open-framework structure with La:Cu molar ratio 2:3 is thus constructed (Figure 2a), which can be described as a cubic 3-connected 10-gon (10,3) net adopting a typical $SrSi_2$ topology with $La(O_2Cu_{1/2})_3$ decorating the vertices of the Si net of $SrSi_2$.[18] A simplified view of the topology containing uniform 2_1 helical channels, in which the $Cu(C_5H_4NPO_3)_2$ units are regarded as linkers and the La atoms as nodes, is shown in Figure 2b. These helical channels are filled with lattice water molecules. The solvent-accessible volume per unit cell is 8.4% in compound **1·La**, as calculated by the PLATON program.[19]

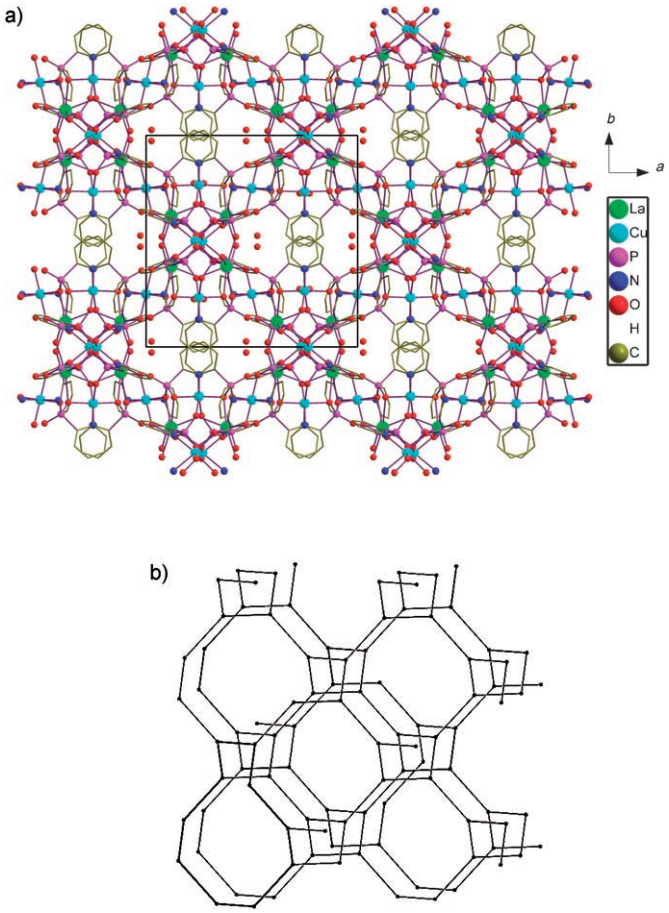

Figure 2. a) Three-dimensional structure of **1·La.** All H atoms are omitted for clarity. b) Simplified view of the topology of **1·La** in which the Cu-$(C_5H_4NPO_3)_2$ units are regarded as linkers and the La atoms as nodes.

The structures of compounds **1·Ln** (Ln = Ce, Pr, Nd) are identical to that of **1·La** except that the cell volumes decrease in the sequence **1·La** > **1·Ce** > **1·Pr** > **1·Nd** due to the effect of the lanthanide contraction. The dihedral angles δ between the CuO1O2E and LnO1O2E planes are 17.2° for **1·Ce**, 16.8° for **1·Pr**, and 17.0° for **1·Nd**. The Cu···Ln distances over the μ-O bridge are 3.733, 3.728, and 3.725 Å for **1·Ce**, **1·Pr**, and **1·Nd**, respectively. Bulk samples of **1·Ln** are racemic because of the presence of equal numbers of right- and left-handed crystals, although single crystals of each compound are chiral.

As far as we are aware, compounds **1·Ln** are the first examples of lanthanide–transition metal heterometallic compounds containing phosphonate ligands. These compounds also provide the first examples of lanthanide complexes that show a chiral open-framework structure. A similar structure has been reported in a few monometallic coordination polymers, which include $[Ag(hmt)](PF_6)\cdot H_2O$,[20a] $[Fe^{II}(2,2'\text{-bipy})_3][Fe^{II}_2(ox)_3]$,[20b] $[Ag_2(2,3\text{-}Me_2pyz)_3](SbF_6)_2$,[20c] $Zn_2(BTC)(NO_3)(H_2O)(C_2H_5OH)_5$,[20d] and [5-(4-ethynylpyridine)pyrimidine]$AgBF_4$.[20e]

*$[Ln_2Cu_3(C_5H_4NPO_3)_6]$ (**2·Ln**; Ln = Pr, Nd, Sm, Eu, Gd, Tb, Dy, Ho)*: Compounds **2·Ln** are isostructural and crystallize in trigonal space group $R\bar{3}$. The asymmetric unit contains two types of Ln atoms (each with 1/6 occupancy), 1/2 Cu atoms, and one 2-pyPO$_3^{2-}$ ligand. Taking **2·Sm** as an example, Figure 3 shows the building block of this structure with

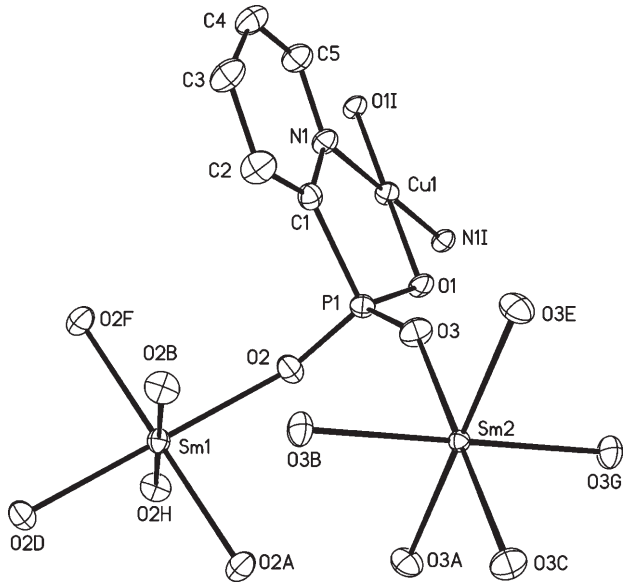

Figure 3. Building block of structure **2·Sm** with atomic labeling scheme (thermal ellipsoids at 30% probability). Symmetry codes: A: $1-y, x-y, z$; B: $1-x+y, 1-x, z$; C: $4/3-x, 2/3-y, -1/3-z$; D: $4/3-x, 2/3-y, 2/3-z$; E: $1/3+y, 2/3-x+y, -1/3-z$; F: $1/3+y, 2/3-x+y, 2/3-z$; G: $1/3+x-y, -1/3+x, -1/3-z$; H: $1/3+x-y, -1/3+x, 2/3-z$; I: $5/3-x, 1/3-y, 1/3-z$.

atomic labeling scheme. The Sm atoms sit on the threefold axes. Each Sm atom is coordinated to six equivalent O atoms from six equivalent phosphonate groups with a distorted octahedral geometry. The Sm1–O2 and Sm2–O3 distances are 2.278(3) and 2.306(3) Å, respectively. The Cu1 atom lies on an inversion center and has a square-planar geometry with four positions occupied by O1, O1I, N1, and N1I from two equivalent 2-pyPO_3^{2-} ligands. The Cu–N and Cu–O distances are 1.902(3) and 1.978(4) Å, respectively.

Each 2-pyPO_3^{2-} again serves as a tetradentate chelating and bridging ligand. In this case, however, the three phosphonate oxygen atoms are each coordinated to a single metal atom (Cu or Sm). The Sm1 and Sm2 atoms are triply bridged by three equivalent O-P-O units to form an infinite chain along the *c* axis with a neighboring Sm1···Sm2 distance of 5.121 Å (Figure 4). Each chain is surrounded by its six

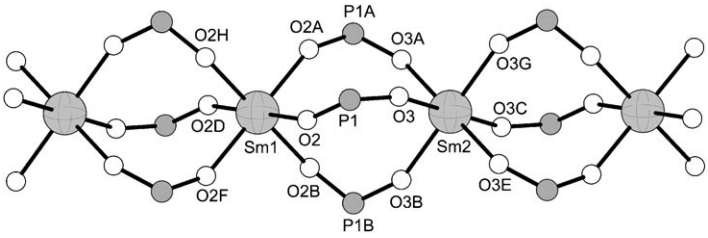

Figure 4. One-dimensional chain of Sm atoms bridged by O-P-O units.

equivalents through corner sharing of {$CuPO_3$} tetrahedra and {CuN_2O_2} planes, and this leads to a three-dimensional framework structure in which the metal atoms are connected purely by O-P-O units (Figure 5). The Cu1···Sm1 and Cu1···Sm2 distances over the O-P-O bridge are 5.674 and 6.398 Å, respectively.

The structures of compounds **2·Ln** (Ln = Pr, Nd, Eu, Gd, Tb, Dy, Ho) are analogous to that of **2·Sm** except that the cell volumes decrease in the sequence **2·Pr** > **2·Nd** > **2·Sm** > **2·Eu** ≈ **2·Gd** > **2·Tb** > **2·Dy** > **2·Ho**, in accordance with the effect of the lanthanide contraction. The average Ln–O bond length also decreases in the same sequence (see Table 5 below).

*$[Ln_2Zn_3(C_5H_4NPO_3)_6]\cdot 4H_2O$ (**Ln_2Zn_3**; Ln = Ce, Pr, Nd)*: The single-crystal structure of **Nd_2Zn_3** is analogous to that of **1·Nd** except that the Cu atoms in the latter are replaced by Zn atoms. Thus, the Nd atom in **Nd_2Zn_3** is also nine-coordinate with Nd–O distances (2.377(7)–2.779(7) Å) slightly longer than those in **1·Nd** (2.346(8)–2.765(9) Å). The Zn–O and Zn–N bond lengths of 1.976(7)–2.125(7) and 2.274(8) Å, respectively, are also comparable to the Cu–O(N) distances in **1·Nd**. The Zn···Nd separation across the μ_3-O bridge is 3.738 Å, while the Zn···Nd, Nd···Nd, and Zn···Zn distances across the O-P-O units are 6.589, 5.756, and 5.950 Å, respectively. Within the NdO_2Zn four-membered ring, the Zn1-O1-Nd1 and Zn1-O2E-Nd1 bond angles are 102.3(3) and 106.0(3)°, respectively. The dihedral angle between the Zn1O1O2E and Nd1O1O2E planes is 17.2°. The XRD data confirm that compounds **Ln_2Zn_3** (Ln = Ce, Pr) are isostructural to **Nd_2Zn_3** and **1·Ln** (Ln = Ce, Pr, Nd) (see the Supporting Information).

*Comparison of structures **1·Ln** and **2·Ln***: By hydrothermal reactions of lanthanide(III) nitrates, copper salts, and 2-pyridylphosphonic acid at 140 °C, we have obtained a series of Ln^{III}–Cu^{II} compounds with two types of structures, namely, compounds $Ln_2Cu_3(C_5H_4NPO_3)_6\cdot 4H_2O$ (**1·Ln**; Ln = La, Ce, Pr, Nd) and $Ln_2Cu_3(C_5H_4NPO_3)_6$ (**2·Ln**; Ln = Pr, Nd, Sm, Eu, Gd, Tb, Dy, Ho). Although their compositions are similar except for the number of lattice water molecules, their structures are completely different. Compounds **1·Ln** crystallize in chiral cubic space group $I2_13$, and compounds **2·Ln** in trigonal space group $R\bar{3}$. In **1·Ln**, each Ln ion is nine-coordinate with a tricapped triprismatic geometry, while each Cu ion is six-coordinate with an octahedral environment. In **2·Ln**, on the other hand, each Ln atom is six-coordinate with an octahedral geometry, while each Cu atom is four-coordinate with a square-planar geometry. Consequently, a chiral open-framework structure is observed in **1·Ln** in which the {LnO_9} tricapped triprisms share edges with the {CuN_2O_4} octahedra. A more dense framework structure is found in **2·Ln**, in which chains of lanthanide phosphonate

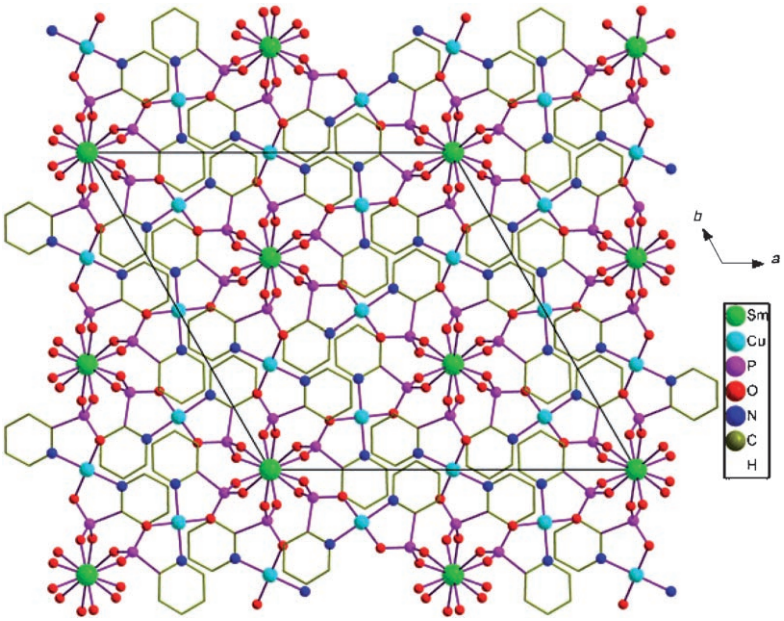

Figure 5. Structure **2·Sm** viewed along the *c* axis. All H atoms are omitted for clarity.

are connected by $\{CuN_2O_2\}$ units. Compounds containing the "light" lanthanide ions La^{3+} and Ce^{3+} show only the first type of structure, whereas compounds containing the "heavy" lanthanide ions Sm^{3+}, Eu^{3+}, Gd^{3+}, Tb^{3+}, Dy^{3+}, and Ho^{3+} exhibit only the second type of structure. For compounds containing the "middle" lanthanide ions Pr^{3+} and Nd^{3+}, both types of structures are observed. Clearly, the effect of the lanthanide contraction plays an important role in formation of a particular structure.

The effect of the coordination capabilities of the copper ion must be considered as well. Because of the Jahn–Teller effect, four-, five-, and six-coordinate modes are all favorable for the Cu^{2+} ion. In compounds **1·Ln** with cubic symmetry, the Cu^{2+} ion is six-coordinate with a slightly distorted octahedral geometry. In compounds **2·Ln** with trigonal symmetry, the Cu^{2+} ion is four-coordinate with a planar geometry. If we replace the Cu^{2+} ion by Zn^{2+}, for which planar coordination is not favorable, only the first type of structure is observed for compounds containing either the light or heavy lanthanide ions.

Differences between compounds containing Cu^{2+} and Zn^{2+} ions: As mentioned above, two types of structures, **1·Ln** with cubic symmetry and **2·Ln** with trigonal symmetry, have been observed for the compounds containing Cu^{2+} ions, while only **1·Ln** has been found for the compounds containing Zn^{2+} ions. We resort to theoretical tools to explain these experimental results.

High computational costs greatly restrict the application of quantum-chemical methods to these complex systems. Small cluster models, which include one metal ion and six nearby 2-pyridylphosphonate molecules, were adopted in our calculations. We studied compounds containing Nd and four-coordinate Zn^{2+}. The central Cu^{2+} ion in the cluster of **2·Ln** was substituted by Zn^{2+}, and the distance was slightly increased because of the larger radius of Zn^{2+}. Different values of total charge (from −4 to 0) were set for clusters containing Cu^{2+} and Zn^{2+}, and the total charge of clusters containing lanthanide ions was taken as −9. Single-point energy calculations were thus performed by employing hybrid DFT with the B3LYP exchange-correlation functional[22,23] and the Gaussian 98 package.[24] The effective core potential (ECP) of Dolg et al. and the related [5s4p3d]-GTO valence basis sets[25] were used for the lanthanides, LANL2DZ[26] for Cu^{2+} and Zn^{2+}, and the 6-31G* basis set for C, H, P, O, and N atoms.

Our computational models of the compounds containing Cu^{2+} and Zn^{2+} are six- and four-coordinate systems, respectively. The calculated values of the energy difference between six- and fourfold coordination ΔE ($E_{6\text{-co}}-E_{4\text{-co}}$) are listed in Table S1. The four-coordinate structure is preferred for Cu^{2+} ($\Delta E=0.17486$ a.u.) but unfavorable for Zn^{2+} (−0.24717 a.u.) with a total charge of −4. Thus, Zn^{2+} only forms the **1·Ln** arrangement, but for Cu^{2+} both **1·Ln** and **2·Ln** structures are possible, because of the Jahn–Teller effect.

*Computational studies on relative stabilities of **1·Ln** and **2·Ln***: To understand the relative thermodynamic stabilities of the configurations of **1·Ln** and **2·Ln** in the Cu^{2+} complex, we carried out both quantum-chemical and molecular mechanics calculations to survey the binding energies and lattice energies of these two structures (Table 1). The B3LYP binding energies of clusters containing Nd was set to be the zero point of both **1·Ln** and **2·Ln** series, as shown in Figure 6a. From Table 1 and Figure 6a, for Pr and Nd **1·Ln** and

Table 1. Lattice energies of **1·Ln**, and **2·Ln** calculated within the framework of MM and PBC model and binding energies of metal ions obtained from DFT calculations.

Metal (r_{Ln} [Å])[a]	Lattice energy [kcal mol^{-1}]		Binding energy [kcal mol^{-1}]	
	1·Ln	**2·Ln**	**1·Ln**	**2·Ln**
La (1.061)	1723.8		12.35	
Ce (1.034)	1727.2		9.98	
Pr (1.013)	1736.9	1664.2	14.83	16.65
Nd (0.995)	1749.6	1672.2	0.0	0.0
Sm (0.964)		1685.2		−2.22
Eu (0.950)		1693.5		−9.31
Gd (0.938)		1700.6		−19.09
Tb (0.923)		1709.6		−24.52
Dy (0.908)		1709.3		−22.63
Ho (0.894)		1726.4		−31.31

[a] Radii of lanthanide ions taken from reference [21].

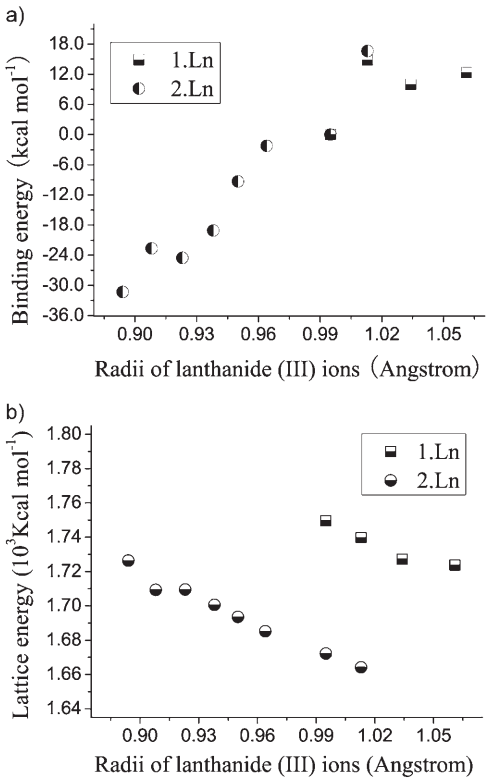

Figure 6. Relationships of a) DFT binding energies and b) calculated lattice energies of **1·Ln** and **2·Ln** with radii of lanthanide ions.

2·Ln have comparable binding energies, in good agreement with the coexistence of both structures in experiment.

Beside the quantum-chemical calculations on the cluster models, we also calculated the lattice energies of the real crystals with the molecular mechanics method. Theoretical models with periodic boundary condition (PBC) were employed to rationalize the differences between **1·Ln** and **2·Ln**, on the basis of the structures obtained from the X-ray crystallographic analysis. The relative stabilities are qualitatively correlated with the relative lattice energies of the two crystal forms. The main intermolecular interactions, that is, electrostatic and van der Waals interactions, are considered in the lattice energy calculations. The charges of lanthanide and copper ions were set to be +3 and +2, respectively. The partial charges of atoms in 2-pyridylphosphonate were derived from CHELPG[27–29] analysis in DFT calculations at the B3LYP[22,23]/6-31G(d) level, and the partial charges of water molecules from the SPC[30] model (−0.82 for O and +0.41 for H). Ewald summation[31] was used to calculate long-range Coulombic interactions and a "spline cutoff" method was adopted to calculate van der Waals interactions. The 12-6 Lennard–Jones parameters were directly derived from the universal force field (UFF).[32–35] All calculations were performed with the OFF module in Cerius2 software.[36]

The calculated lattice energies E_{cryst} of **1·Ln** and **2·Ln** (Table 1) exhibit a nearly linear relationship with the radii of lanthanide ions r_{Ln} [Eq. (1)]

$$E_{cryst} = \alpha r_{Ln} + \beta \quad (1)$$

where the fitted parameters α (β) are −385.1 kcal mol^{-1} Å^{-1} (2067.8 kcal mol^{-1}) and −496.1 kcal mol^{-1} Å^{-1} (2230.0 kcal mol^{-1}) for **1·Ln** and **2·Ln**, respectively. The correlations of the lattice energies with the radii of metal ions, depicted in Figure 6b, are in line with the principle of lanthanide contraction. Obviously, differences between the structures of the **1·Ln** and **2·Ln** lead to different lattice energies. For the ions La and Ce with larger radii, lattice energies of **1·Ln** conformers are larger than those of **2·Ln**, and hence **1·Ln** is preferred. This is easily understood since the ion with larger radius favors a higher coordination number and a larger cavity to accommodate more water molecules.

Magnetic properties: The variable-temperature magnetic susceptibility data for compounds **1·Ln** (Ln = La, Ce, Pr, Nd) and **2·Ln** (Ln = Sm, Eu, Gd, Tb, Dy, Ho) were measured in the temperature range 1.8–300 K in an applied magnetic field of 2 kG. Figure 7 shows the $\chi_M T$ versus T plot for compounds **1·Ln**. The $\chi_M T$ value of **1·La** is 1.42 cm^3 K mol^{-1} at room temperature, slightly higher than the calculated spin-only value (1.24 cm^3 K mol^{-1}) for three uncoupled S = 1/2 spins of Cu^{II} ions (g = 2.1) since no contribution is expected for the nonmagnetic La^{III} ions. On cooling, the $\chi_M T$ value remains essentially constant down to about 55 K, below which it increases sharply to 2.05 cm^3 K mol^{-1} at 1.8 K. The Curie–Weiss fitting of the magnetic data over the whole temperature range 2–300 K

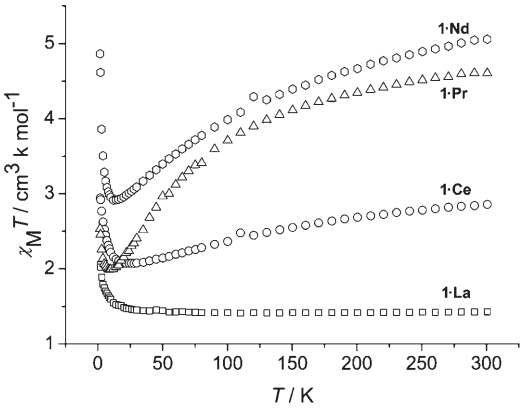

Figure 7. Plots of $\chi_M T$ versus T for **1·Ln**.

results in a Curie constant C = 1.42 cm^3 K mol^{-1} and a Weiss constant θ = 0.63 K, characteristic of a very weak ferromagnetic interaction between the Cu^{II} centers. The magnetization measured at 1.8 K for **1·La** shows that the saturation value at 70 kG is 3.21 $N\beta$, close to the value of 3.15 $N\beta$ expected for three Cu^{2+} ions with g = 2.1 (see Supporting Information). No long-range magnetic ordering is observed down to 1.8 K.

For **1·Ce**, **1·Pr**, and **1·Nd**, the room-temperature $\chi_M T$ values are 2.72, 4.60, and 5.06 cm^3 K mol^{-1}, respectively, close to the theoretical values (2.73, 4.33, and 4.41 cm^3 K mol^{-1}) for three isolated Cu^{II} and two isolated Ln^{III} ions. On cooling, the $\chi_M T$ values decrease continuously and reach minima at 26, 9, and 12 K for **1·Ce** (2.06 cm^3 K mol^{-1}), **1·Pr** (2.00 cm^3 K mol^{-1}), and **1·Nd** (2.92 cm^3 K mol^{-1}), respectively. Below these temperatures, the $\chi_M T$ values increase sharply and approach 2.94, 2.53, and 4.86 cm^3 K mol^{-1} for **1·Ce**, **1·Pr**, and **1·Nd**, respectively, at 1.8 K (Figure 7).

From the structure of **1·Ln**, it is clear that the magnetic interactions between Ln^{III} and Cu^{II} may be mediated through two pathways: one through the μ-O bridge and the other through the O-P-O unit, while the interaction between the same metal ions, that is, Ln^{III}–Ln^{III} and Cu^{II}–Cu^{II}, can be propagated only through O-P-O units. For compound **1·La**, which contains diamagnetic La^{III} ions, the overall ferromagnetic behavior is attributed to Cu^{II}–Cu^{II} exchange coupling via O-P-O bridges. Ferromagnetic phenomena have already been observed in a few copper phosphonate compounds in which the Cu^{II} ions are connected purely through O-P-O bridges.[37]

For compounds **1·Ce**, **1·Pr**, and **1·Nd**, both the Ln^{III}–Cu^{II} and Ln^{III}–Ln^{III} interactions must be considered besides the Cu^{II}–Cu^{II} interactions. Furthermore, the Ce^{III}, Pr^{III}, and Nd^{III} ions have ground states of $^2F_{5/2}$, $^3H_4$, and $^4I_{9/2}$, respectively. The first-order orbital momentum and thus the spin–orbital couplings of the single lanthanide ions must be considered, which makes understanding the magnetic behaviors of these complexes more difficult. To understand the nature of the Ln^{III}–Cu^{II} interactions in **1·Ce**, **1·Pr**, and **1·Nd**, the Ln^{III}–Ln^{III} and Cu^{II}–Cu^{II} interactions mediated through the O-P-O

units must be circumvented. Since the structure of compounds $\mathbf{Ln_2Zn_3}$ are identical to those of **1·Ln**, the Ln^{III}–Ln^{III} interaction in $\mathbf{Ln_2Zn_3}$ should be similar to that in the corresponding compound **1·Ln**. While the Cu^{II}–Cu^{II} interaction across the O-P-O unit is considered to be analogous to that in **1·La**. Consequently, the contribution of the Ln^{III}–Cu^{II} interaction to the overall magnetic susceptibility can be obtained simply by the equation $\Delta = (\chi_M T)_{\mathbf{1\cdot Ln}} - (\chi_M T)_{\mathbf{Ln2Zn3}} - (\chi_M T)_{\mathbf{1\cdot La}}$.

Figure 8 shows $\chi_M T$ versus T curves for compounds **1·Ce**, $\mathbf{Ce_2Zn_3}$, and **1·La**. The Δ versus T curve, attributed to the Ce^{III}–Cu^{II} interactions in **1·Ce**, can be approximately obtained by subtracting the contributions of Ce^{III}–Ce^{III} and Cu^{II}–Cu^{II} interactions from $\mathbf{Ce_2Zn_3}$ and **1·La**, respectively. On cooling from room temperature, Δ remains almost constant and close to zero down to 50 K. Below 50 K, Δ increases rapidly with decreasing T. The profile of the Δ versus T curve is characteristic of ferromagnetic interactions between Ce^{III} and Cu^{II} ions. Similarly, the Pr^{III}–Cu^{II} and Nd^{III}–Cu^{II} interactions are also found to be ferromagnetic (see Supporting Information). This result, however, is in contrast with the prediction that the Ln^{III}–Cu^{II} interaction is antiferromagnetic for Ln^{III} ions with fewer than seven 4f electrons.

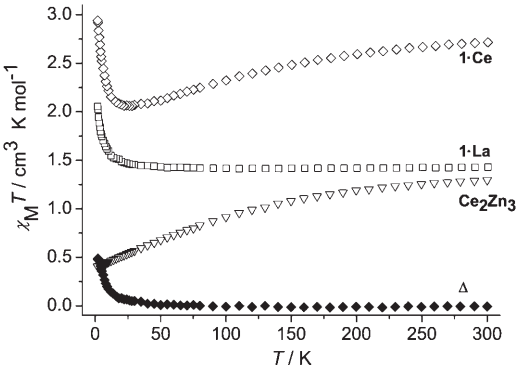

Figure 8. Plots of $\chi_M T$ versus T for **1·Ce**, **1·La**, and $\mathbf{Ce_2Zn_3}$. $\Delta = (\chi_M T)_{\mathbf{1\cdot Ce}} - (\chi_M T)_{\mathbf{Ce2Zn3}} - (\chi_M T)_{\mathbf{1\cdot La}}$.

Figure 9 shows the $\chi_M T$ versus T plots for compounds **2·Ln** (Ln = Sm, Eu, Gd, Tb, Dy, Ho). According to their structures, two magnetic exchange pathways are possible for propagating the magnetic interactions in **2·Ln**: Ln^{III}–Cu^{II} interactions and Ln^{III}–Ln^{III} interactions through the O-P-O units. Since Gd^{III} has no orbital angular momentum, the magnetic behavior of **2·Gd** can be easily interpreted. As shown in Figure 9, the room-temperature $\chi_M T$ value for **2·Gd** (16.81 $cm^3 K mol^{-1}$) is close to the spin-only value of 16.89 $cm^3 K mol^{-1}$ expected for three isolated Cu^{II} and two isolated Gd^{III} ions. It remains almost constant down to about 30 K, below which the $\chi_M T$ value decreases with decreasing temperature. The decline in $\chi_M T$ at low temperature can be attributed to antiferromagnetic exchange coupling between the magnetic centers across the O-P-O units. Since the O-P-O unit is not efficient in mediating magnetic exchange due to electron localization, the overall antiferromagnetic interaction in **2·Gd** would be expected to be very weak. This is indeed the case. The χ_M^{-1} versus T curve shows that the magnetic susceptibility data follow the Curie–Weiss law in the whole temperature range with a Curie constant $C = 16.88\ cm^3 K mol^{-1}$ and a Weiss constant $\theta = -0.61$ K (see Supporting Information).

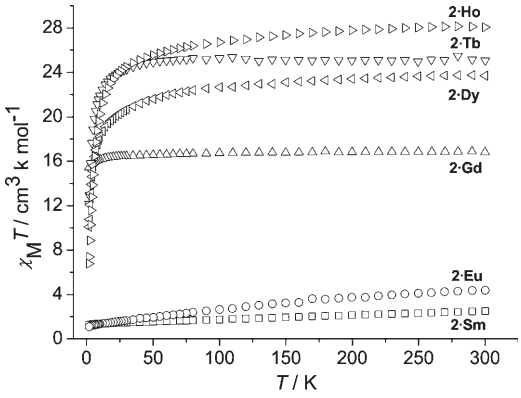

Figure 9. Plots of $\chi_M T$ versus T for **2·Ln** (Ln = Sm, Eu, Gd, Tb, Dy, Ho).

For compounds **2·Ln** containing the lanthanide ions Sm^{III}, Eu^{III}, Tb^{III}, Dy^{III}, and Ho^{III}, the contributions of the single-ion orbital-momentum must be considered. Hence, the room-temperature $\chi_M T$ values for **2·Sm** (2.51 $cm^3 K mol^{-1}$) and **2·Eu** (4.40 $cm^3 K mol^{-1}$) are larger than those expected from the free-ion approximation (1.31 and 1.125 $cm^3 K mol^{-1}$, respectively), owing to the presence of thermally populated excited states of Sm^{III} and Eu^{III} ions. The magnetic behaviors of **2·Sm** and **2·Eu** are characterized by continuously decreasing $\chi_M T$ on cooling, mainly due to thermal depopulation of the excited states.

For **2·Ln** (Ln = Tb, Dy, Ho), the room-temperature $\chi_M T$ values are 25.08 $cm^3 K mol^{-1}$ for **2·Tb**, 28.06 $cm^3 K mol^{-1}$ for **2·Ho**, and 23.71 $cm^3 K mol^{-1}$ for **2·Dy**. The values are close to the expected values of 24.77 $cm^3 K mol^{-1}$ for **2·Tb** and 29.27 $cm^3 K mol^{-1}$ for **2·Ho**, but lower than that for **2·Dy** (29.47 $cm^3 K mol^{-1}$). On cooling, the $\chi_M T$ values remain essentially constant from 300 to about 50 K in all cases, below which $\chi_M T$ decreases continuously. Such magnetic behaviors could originate from the combined contributions of antiferromagnetic interactions between the magnetic centers and the spin–orbital couplings of the single lanthanide ions.

Conclusion

By using the unsymmetrical ligand 2-pyridylphosphonate, we have obtained the first 3d–4f heterometallic phosphonate compounds $Ln_2Cu_3(C_5H_4NPO_3)_6 \cdot 4H_2O$ (**1·Ln**; Ln = La, Ce, Pr, Nd) and $Ln_2Cu_3(C_5H_4NPO_3)_6$ (**2·Ln**; Ln = Pr, Nd, Sm, Eu, Gd, Tb, Dy, Ho). Compounds **1·Ln** are rare examples of 3d–4f complexes that form a chiral open-framework structure with a 3-connected 10-gon (10,3) topology, while compounds **2·Ln** are centrosymmetric with a more con-

densed 3D structure. The remarkable differences between structures **1·Ln** and **2·Ln** are ascribable to the effect of the lanthanide contraction as well as the coordinative versatility of the Cu^{2+} ion, as was rationalized by theoretical calculations. The magnetic properties of complexes **1·Ln** and **2·Ln** were investigated. In **1·Ln**, the nature of the Ln^{III}–Cu^{II} (Ln = Ce, Pr, Nd) interactions could be elucidated by subtracting the contributions of Ln^{III}–Ln^{III} and Cu^{II}–Cu^{II} interactions. The latter can be approximately obtained by measuring the magnetic susceptibilities of compounds **Ln_2Zn_3** and **1·La**, respectively. Surprisingly, the results demonstrate that the Ln^{III}–Cu^{II} (Ln = Ce, Pr, Nd) interactions in **1·Ln** are ferromagnetic, opposite to the prediction of antiferromagnetic coupling for Ln^{III} ions with fewer than seven 4f electrons. Further work is in progress to understand the nature of the Ln^{III}–M^{II} interactions.

Experimental Section

Materials and methods: All starting materials were of reagent grade and used as purchased. 2-Pyridylphosphonic acid (2-$C_5H_4NPO_3H_2$, 2-pyPO_3H_2) was prepared according to the literature.[38] Elemental analyses were performed on a PE 240C elemental analyzer. The infrared spectra were recorded on a VECTOR 22 spectrometer with pressed KBr pellets. Thermal analyses were performed in nitrogen with a heating rate of 20 °C min^{-1} on a Perkin Elmer Pyris 1 TGA instrument. Magnetic susceptibility was measured on polycrystalline samples by using a Quantum Design MPMS-XL7 SQUID magnetometer. The magnetic data were corrected for the diamagnetic contributions of both the sample holder and the compound obtained from Pascal's constants.[39]

Preparation of $[Ln_2Cu_3(C_5H_4NPO_3)_6]\cdot 4H_2O$ (1·Ln; Ln = La, Ce, Pr, Nd): These compounds were prepared by a similar experimental procedure except that appropriate lanthanide(III) nitrate hydrates were used. A typical procedure for the preparation of **1·La** is described. A mixture of 2-py$PO_3H_2\cdot H_2O$ (0.1 mmol, 0.0177 g), $Cu(O_2CCH_3)_2\cdot H_2O$ (0.05 mmol, 0.010 g), $La(NO_3)_3\cdot 6H_2O$ (0.033 mmol, 0.0144 g), and H_2O (8.0 mL) was transferred to a Teflon-lined autoclave and heated at 140 °C for two days. The pale blue cubic crystals were collected, washed with H_2O, and dried in air. Yield: 11 mg (45 % based on La). Elemental analysis (%) calcd for $C_{30}H_{24}N_6O_{18}P_6Cu_3La_2\cdot 4H_2O$: C 24.30, H 2.18, N 5.67; found: C 24.40, H 2.28, N 5.81; IR (KBr): $\tilde{\nu}$ = 3447(br), 1654(w), 1639(w), 1593(w), 1581(w), 1458(w), 1421(w), 1279(w), 1176(m), 1130(s), 1063(s), 1029(s), 972(s), 780(m), 736(m), 594(s), 564(m), 536(m) cm^{-1}.

1·Ce: Yield 10 mg (40 % based on Ce). Elemental analysis (%) calcd for $C_{30}H_{24}N_6O_{18}P_6Cu_3Ce_2\cdot 4H_2O$: C 24.26, H 2.17, N 5.66; found: C 24.19, H 2.17, N 5.66; IR (KBr): $\tilde{\nu}$ = 3528(br), 1654(w), 1639(w), 1593(w), 1582(w), 1461(w), 1429(w), 1280(w), 1178(m), 1132(s), 1063(s), 1026(s), 974(s), 778(m), 736(m), 594(s), 565(m), 536(m) cm^{-1}.

1·Pr: Yield 12 mg (48 % based on Pr). Elemental analysis (%) calcd for $C_{30}H_{24}N_6O_{18}P_6Cu_3Pr_2\cdot 4H_2O$: C 24.23, H 2.17, N 5.65; found: C 24.75, H 2.01, N 5.83; IR (KBr): $\tilde{\nu}$ = 3529(br), 1653(w), 1640(w), 1593(w), 1582(w), 1461(w), 1422(w), 1279(w), 1177(m), 1130(s), 1063(s), 1027(s), 973(s), 780(m), 736(m), 593(s), 565(m), 537(m) cm^{-1}.

1·Nd: Yield 10 mg (40 % based on Nd). Elemental analysis (%) calcd for $C_{30}H_{24}N_6O_{18}P_6Cu_3Nd_2\cdot 4H_2O$: C 24.12, H 2.16, N 5.63; found: C 24.22, H 2.14, N 5.65; IR (KBr): $\tilde{\nu}$ = 3448(br), 1653(w), 1639(w), 1593(w), 1582(w), 1460(w), 1421(w), 1280(w), 1177(m), 1131(s), 1063(s), 1027(s), 974(s), 779(m), 736(m), 593(s), 564(m), 536(m) cm^{-1}.

Thermal analyses were performed for compounds **1·Ln** (Ln = La, Ce, Pr, Nd). All four experience two-step decomposition between room temperature and 700 °C. The first step starts at about 100 °C and becomes complete before 370 °C. The weight losses are 4.75, 4.67, 4.42, and 4.66 % for **1·La**, **1·Ce**, **1·Pr**, and **1·Nd**, respectively, which are in agreement with the removal of four lattice water molecules (4.86 % for **1·La**, 4.85 % for **1·Ce**, 4.84 % for **1·Pr**, and 4.82 % for **1·Nd**). The second step of decomposition occurs between 400 and 500 °C and corresponds to combustion of the organic moieties of the compounds. The XRD patterns for the hydrated and dehydrated samples of compound **1·La** reveal that the framework structure of **1·La** is maintained after removal of the lattice water molecules (see the Supporting Information).

Preparation of $Ln_2Cu_3(C_5H_4NPO_3)_6$ (2·Ln; Ln = Pr, Nd, Sm, Eu, Gd, Tb, Dy, Ho): These compounds were prepared by following a similar experimental procedure except that an appropriate lanthanide(III) nitrate hydrate was used. A typical procedure for the preparation of **2·Sm** is described. A mixture of 2-py$PO_3H_2\cdot H_2O$ (0.1 mmol, 0.0177 g), $CuSO_4$ (0.05 mmol, 0.008 g), $Sm(NO_3)_3\cdot 6H_2O$ (0.033 mmol, 0.0148 g), and H_2O (8 mL) was transferred to a Teflon-lined autoclave and heated at 140 °C for 2 d. The purple platelike crystals of **2·Sm** were collected, washed with H_2O, and dried in air. Yield: 13 mg (55 % based on Sm). Elemental analysis (%) calcd for $C_{30}H_{24}N_6O_{18}P_6Cu_3Sm_2$: C 25.13, H 1.69, N 5.86; found: C 25.21, H 1.79, N 5.86; IR (KBr): $\tilde{\nu}$ = 1591(w), 1466(w), 1432(w), 1282(w), 1175(m), 1156(s), 1139(s), 1101(s), 1084(s), 1052(m), 988(m), 781(m), 728(m), 626(s), 552(m), 486(w), 422(w) cm^{-1}.

2·Pr: Yield 2 mg (9 % based on Pr). Elemental analysis (%) calcd for $C_{30}H_{24}N_6O_{18}P_6Cu_3Pr_2$: C 25.46, H 1.71, N 5.94; found: C 25.36, H 1.70, N 5.98; IR (KBr): $\tilde{\nu}$ = 1591(w), 1465(w), 1431(w), 1281(w), 1176(m), 1155(s), 1133(s), 1101(s), 1084(s), 1052(m), 987(m), 781(m), 729(m), 627(s), 550(m), 485(w), 421(w) cm^{-1}.

Table 2. Crystallographic data for **1·Ln** and **Nd_2Zn_3**.

Compound	**1·La**	**1·Ce**	**1·Pr**	**1·Nd**	**Nd_2Zn_3**
formula	$C_{30}H_{32}N_6O_{22}P_6\ Cu_3La_2$	$C_{30}H_{32}N_6O_{22}P_6\ Cu_3Ce_2$	$C_{30}H_{32}N_6O_{22}P_6\ Cu_3Pr_2$	$C_{30}H_{32}N_6O_{22}P_6\ Cu_3Nd_2$	$C_{30}H_{32}N_6O_{22}P_6\ Zn_3Nd_2$
M	1482.88	1485.30	1486.88	1493.54	1499.03
crystal dimensions [mm^3]	0.28 × 0.24 × 0.24	0.28 × 0.24 × 0.24	0.28 × 0.24 × 0.24	0.30 × 0.28 × 0.28	0.30 × 0.26 × 0.24
crystal system	cubic	cubic	cubic	cubic	cubic
space group	$I2_13$	$I2_13$	$I2_13$	$I2_13$	$I2_13$
a [Å]	16.280(1)	16.238(2)	16.211(2)	16.175(2)	16.266(1)
V [Å^3]	4314.7(3)	4281.2(7)	4260.0(11)	4231.5(9)	4303.6(4)
Z	4	4	4	4	4
ρ_{calcd} [g cm^{-3}]	2.283	2.304	2.318	2.344	2.314
$F(000)$	2884	2892	2900	2908	2920
μ [mm^{-1}]	3.708	3.868	4.037	4.216	4.335
GoF on F^2	1.128	1.105	1.142	1.136	1.062
R_1, wR_2[a] [$I > 2\sigma(I)$]	0.0474, 0.0968	0.0421, 0.0928	0.0404, 0.0809	0.0565, 0.1254	0.0441, 0.1077
R_1, wR_2[a] (all data)	0.0529, 0.0984	0.0469, 0.0941	0.0456, 0.0820	0.0603, 0.1268	0.0492, 0.1093
$(\Delta\rho)_{max}$, $(\Delta\rho)_{min}$ [e Å^{-3}]	0.435, −0.660	0.632, −1.163	0.403, −0.950	0.88, −1.012	0.77, −1.17

[a] $R_1 = \Sigma||F_o| - |F_c||/\Sigma|F_o|$; $wR_2 = [\Sigma w(F_o^2 - F_c^2)^2/\Sigma w(F_o^2)^2]^{1/2}$.

Table 3. Crystallographic data for **2·Ln**.

Compound	**2·Pr**	**2·Nd**	**2·Sm**	**2·Eu**	**2·Gd**	**2·Tb**	**2·Dy**	**2·Ho**
formula	$C_{30}H_{24}N_6O_{18}P_6Cu_3Pr_2$	$C_{30}H_{24}N_6O_{18}P_6Cu_3Nd_2$	$C_{30}H_{24}N_6O_{18}P_6Cu_3Sm_2$	$C_{30}H_{24}N_6O_{18}P_6Cu_3Eu_2$	$C_{30}H_{24}N_6O_{18}P_6Cu_3Gd_2$	$C_{30}H_{24}N_6O_{18}P_6Cu_3Tb_2$	$C_{30}H_{24}N_6O_{18}P_6Cu_3Dy_2$	$C_{30}H_{24}N_6O_{18}P_6Cu_3Ho_2$
M	1414.81	1421.47	1433.69	1436.91	1447.49	1450.83	1457.99	1462.85
crystal dimensions [mm^3]	0.32×0.28×0.28	0.32×0.26×0.24	0.32×0.26×0.24	0.30×0.26×0.24	0.32×0.28×0.26	0.30×0.26×0.24	0.30×0.26×0.24	0.30×0.26×0.26
crystal system	trigonal	trigonal	trigonal	trigonal	trigonal	trigonal	trigonal	trigonal
space group	$R\bar{3}$	$R\bar{3}$	$R\bar{3}$	$R\bar{3}$	$R\bar{3}$	$R\bar{3}$	$R\bar{3}$	$R\bar{3}$
a [Å]	18.808(4)	18.818(3)	18.744(3)	18.724(3)	18.742(3)	18.696(3)	18.678(4)	18.622(3)
c [Å]	10.329(3)	10.310(2)	10.242(2)	10.210(2)	10.191(2)	10.161(2)	10.155(2)	10067(2)
V [Å^3]	3164.3(13)	3161.7(10)	3116.2(10)	3100.1(10)	3100.1(10)	3076.0(9)	3068.0(12)	3023.3(8)
Z	3	3	3	3	3	3	3	3
ρ_{calcd} [g cm^{-3}]	2.227	2.240	2.292	2.309	2.326	2.350	2.367	2.411
$F(000)$	2055	2061	2073	2079	2085	2091	2097	2103
μ [mm^{-1}]	4.064	4.219	4.608	4.825	4.999	5.253	5.462	5.762
GoF on F^2	1.265	1.040	0.981	1.124	0.977	0.938	1.069	1.232
R_1, wR_2[a] [$I>2\sigma(I)$]	0.0454, 0.1328	0.0374, 0.0958	0.0256, 0.0468	0.022, 0.0576	0.0267, 0.0523	0.0288, 0.0550	0.0346, 0.0696	0.0460, 0.1054
R_1, wR_2[a] (all data)	0.0495, 0.1352	0.0454, 0.0988	0.0336, 0.0485	0.0242, 0.0585	0.0358, 0.0543	0.0392, 0.0574	0.0431,-0.0730	0.0653, 0.1099
$(\Delta\rho)_{max}$, $(\Delta\rho)_{min}$ [e Å^{-3}]	3.486, −3.755	3.145, −1.145	0.516, −0.412	0.669, −0.697	0.714, −0.520	1.030, −0.459	1.259, −0.490	1.077, −1.134

[a] $R_1=\Sigma||F_o|-|F_c||/\Sigma|F_o|$; $wR_2=[\Sigma w(F_o^2-F_c^2)^2/\Sigma w(F_o^2)^2]^{1/2}$.

2·Nd: Yield 5 mg (23% based on Nd). Elemental analysis (%) calcd for $C_{30}H_{24}N_6O_{18}P_6Cu_3Nd_2$: C 25.35, H 1.70, N 5.91; found: C 25.35, H 1.69, N 5.87; IR (KBr): $\tilde{\nu}$=1591(w), 1465(w), 1432(w), 1281(w), 1175(m), 1155(s), 1136(s), 1101(s), 1083(s), 1052(m), 988(m), 780(m), 729(m), 627(s), 551(m), 486(w), 422(w) cm^{-1}.

Table 4. Selected bond lengths [Å] and angles [°] for **1·Ln** and **Nd_2Zn_3**.[a]

	1·La	**1·Ce**	**1·Pr**	**1·Nd**	**Nd_2Zn_3**
Ln1−O1	2.778(5)	2.780(5)	2.763(5)	2.765(9)	2.779(7)
Ln1−O2	2.545(5)	2.536(5)	2.517(5)	2.489(10)	2.546(7)
Ln1−O3B	2.415(5)	2.378(5)	2.366(5)	2.346(8)	2.377(7)
M1−O1	1.965(5)	1.971(5)	1.964(5)	1.972(10)	1.976(7)
M1−N1	2.180(7)	2.260(8)	2.229(7)	2.194(11)	2.274(8)
M1−O2D	2.137(5)	2.136(5)	2.137(5)	2.136(10)	2.125(7)
P1−O1	1.536(6)	1.520(5)	1.535(5)	1.511(9)	1.520(7)
P1−O2	1.545(5)	1.533(5)	1.541(5)	1.548(10)	1.543(7)
P1−O3	1.498(5)	1.507(5)	1.504(5)	1.517(9)	1.517(7)
O1-Ln1-O2	55.25(15)	55.15(15)	55.63(15)	55.4(3)	55.4(2)
O1-Ln1-O1E	115.21(14)	115.57(14)	115.73(14)	115.7(3)	115.6(2)
O1-Ln1-O3B	78.69(15)	77.82(16)	77.47(16)	79.8(3)	79.6(2)
O1-Ln1-O3C	152.88(15)	152.45(16)	152.43(16)	152.0(3)	152.3(2)
O1-Ln1-O3D	74.52(16)	74.59(16)	74.42(16)	75.1(3)	74.8(2)
O1-Ln1-O2E	62.55(15)	63.17(15)	63.01(15)	63.1(3)	62.9(2)
O1-Ln1-O2F	127.17(15)	128.04(15)	128.20(15)	128.2(3)	128.2(2)
O2-Ln1-O3B	79.95(16)	79.52(16)	79.37(16)	79.8(3)	79.6(2)
O2-Ln1-O3C	140.61(16)	140.28(16)	139.85(16)	139.8(3)	139.9(2)
O2-Ln1-O3D	129.15(16)	129.18(16)	129.53(16)	129.9(3)	129.6(2)
O2-Ln1-O2E	83.42(16)	84.01(16)	83.86(16)	84.1(3)	84.2(2)
O3B-Ln1-O3C	83.39(16)	83.42(17)	83.72(17)	82.9(3)	83.1(2)
O1-M1-N1	83.8(2)	83.0(2)	83.3(2)	84.7(4)	83.1(3)
O1-M1-O1A	176.5(2)	177.1(2)	175.8(2)	176.4(4)	176.9(3)
O1-M1-N1A	98.9(2)	99.3(2)	99.9(2)	98.1(4)	99.2(3)
O1-M1-O2D	92.7(2)	92.4(2)	92.3(2)	93.2(4)	92.4(3)
O1-M1-O2E	84.9(2)	85.57(19)	84.77(19)	84.3(4)	85.5(3)
N1-M1-N1A	79.3(2)	79.3(3)	79.8(2)	79.4(4)	79.4(4)
O2D-M1-N1	172.5(2)	171.9(2)	172.2(2)	173.6(4)	172.0(3)
O2E-M1-N1	94.8(2)	95.0(2)	94.6(2)	95.0(4)	94.9(3)
O2D-M1-O2E	91.48(19)	91.23(19)	91.46(19)	90.8(4)	91.3(3)
Ln1-O1-M1	103.1(2)	102.2(2)	102.8(2)	102.4(4)	102.3(3)
Ln1-O2E-M1	106.0(2)	105.8(2)	106.2(2)	107.1(4)	106.0(3)

[a] Symmetry codes: A: 1−x, 3/2−y, z; B: x, 1−y, 1/2−z; C: 1−x, 1/2−y, z; D: y, 1−z, 1/2−x; E: 1−y, 1/2+z, 1/2−x; F: 1/2−z, 1−x, −1/2+y.

2·Eu: Yield 12 mg (50% based on Eu). Elemental analysis (%) calcd for $C_{30}H_{24}N_6O_{18}P_6Cu_3Eu_2$: C 25.08, H 1.68, N 5.85; found: C 25.11, H 1.72, N 5.85; IR (KBr): $\tilde{\nu}$=1592(w), 1466(w), 1433(w), 1283(w), 1176(m), 1156(s), 1142(s), 1103(s), 1084(s), 1052(m), 990(m), 781(m), 728(m), 625(s), 555(m), 487(w), 424(w) cm^{-1}.

2·Gd: Yield 11 mg (46% based on Gd). Elemental analysis (%) calcd for $C_{30}H_{24}N_6O_{18}P_6Cu_3Gd_2$: C 24.89, H 1.67, N 5.81; found: C 24.88, H 1.79, N 5.63; IR (KBr): $\tilde{\nu}$=1592(w), 1466(w), 1432(w), 1282(w), 1175(m), 1156(s), 1140(s), 1101(s), 1085(s), 1053(m), 989(m), 781(m), 728(m), 625(s), 553(m), 486(w), 423(w) cm^{-1}.

2·Tb: Yield 12 mg (50% based on Tb). Elemental analysis (%) calcd for $C_{30}H_{24}N_6O_{18}P_6Cu_3Tb_2$: C 24.83, H 1.67, N 5.79; found: C 24.87, H 1.73, N 5.61; IR (KBr): $\tilde{\nu}$=1592(w), 1466(w), 1433(w), 1282(w), 1176(m), 1156(s), 1142(s), 1102(s), 1087(s), 1052(m), 990(m), 781(m), 728(m), 625(s), 554(m), 487(w), 423(w) cm^{-1}.

2·Dy: Yield 13 mg (54% based on Dy). Elemental analysis (%) calcd for $C_{30}H_{24}N_6O_{18}P_6Cu_3Dy_2$: C 24.71, H 1.66, N 5.76; found: C 24.77, H 1.69, N 5.60; IR (KBr): $\tilde{\nu}$=1592(w), 1466(w), 1433(w), 1282(w), 1176(m), 1156(s), 1142(s), 1102(s), 1087(s), 1052(m), 990(m), 781(m), 728(m), 625(s), 554(m), 487(w), 423(w) cm^{-1}.

2·Ho: Yield 11 mg (45% based on Ho). Elemental analysis (%) calcd for

Table 5. Selected bond lengths [Å] and angles [°] for **2·Ln**.[a]

	2·Pr	2·Nd	2·Sm	2·Eu	2·Gd	2·Tb	2·Dy	2·Ho
Ln1−O2	2.308(6)	2.296(6)	2.278(3)	2.268(3)	2.256(3)	2.245(3)	2.240(4)	2.203(7)
Ln(2)−O3	2.354(6)	2.340(5)	2.306(3)	2.295(3)	2.294(4)	2.270(3)	2.270(4)	2.245(7)
Cu1−O1	1.898(5)	1.902(4)	1.902(3)	1.902(2)	1.907(3)	1.910(3)	1.905(4)	1.903(7)
Cu1−N1	1.985(6)	1.987(6)	1.978(4)	1.983(3)	1.982(3)	1.985(4)	1.985(5)	1.992(10)
P1−O1	1.520(7)	1.531(5)	1.519(3)	1.526(3)	1.519(3)	1.523(3)	1.518(4)	1.514(9)
P1−O2	1.492(5)	1.491(5)	1.497(3)	1.494(2)	1.503(4)	1.501(3)	1.497(4)	1.484(7)
P1−O3	1.486(6)	1.493(5)	1.496(3)	1.495(2)	1.496(3)	1.501(4)	1.499(4)	1.499(7)
O2-Ln1-O2	87.49(19)	87.74(19)	88.19(10)	88.23(9)	88.67(13)	88.71(13)	88.51(15)	88.7(3)
O3-Ln2-O3A	90.65(19)	90.56(19)	90.53(10)	90.31(10)	90.61(13)	90.36(13)	90.34(13)	90.7(3)
O1-Cu1-N1	88.0(2)	88.10(19)	87.75(13)	87.92(11)	87.73(14)	87.81(15)	87.61(19)	88.1(3)

[a] Symmetry transformations used to generate equivalent atoms: A: $1-y, x-y, z$

$C_{30}H_{24}N_6O_{18}P_6Cu_3Ho_2$: C 24.63, H 1.65, N 5.74; found: C 24.73, H 1.71, N 5.69; IR (KBr): $\tilde{\nu}$ = 1592(w), 1466(w), 1433(w), 1283(w), 1176(m), 1156(s), 1142(s), 1103(s), 1087(s), 1052(m), 990(m), 781(m), 728(m), 625(s), 555(m), 487(w), 423(w) cm^{-1}.

Preparation of $[Ln_2Zn_3(C_5H_4NPO_3)_6]\cdot 4H_2O$ (Ln_2Zn_3; Ln = Ce, Pr, Nd): These compounds were prepared by an experimental procedure similar to that described for **1·La**, except that the appropriate lanthanide(III) nitrate hydrate and zinc sulfate were used.

Ce_2Zn_3: Yield 11 mg (45% based on Ce). Elemental analysis (%) calcd for $C_{30}H_{24}N_6O_{18}P_6Zn_3Ce_2\cdot 4H_2O$: C 24.17, H 2.16, N 5.64; found: C 24.13, H 2.27, N 5.59; IR (KBr): $\tilde{\nu}$ = 3530(br), 1660(w), 1635(w), 1589(w), 1564(w), 1461(w), 1427(w), 1279(w), 1200(m), 1176(s), 1138(s), 1070(s), 1048(s), 1034(s), 1009(m), 977(s), 779(m), 734(m), 587(s), 562(m), 534(m) cm^{-1}.

Pr_2Zn_3: Yield 13 mg (53% based on Pr). Elemental analysis (%) calcd for $C_{30}H_{24}N_6O_{18}P_6Zn_3Pr_2\cdot 4H_2O$: C 24.14, H 2.16, N 5.63; found: C 24.15, H 2.17, N 5.64; IR (KBr): $\tilde{\nu}$ = 3537(br), 1659(w), 1636(w), 1589(w), 1564(w), 1461(w), 1427(w), 1279(w), 1200(m), 1176(s), 1139(s), 1069(s), 1049(s), 1033(s), 1009(m), 977(s), 779(m), 734(m), 586(s), 563(m), 534(m) cm^{-1}.

Nd_2Zn_3: Yield 14 mg, (57% based on Nd). Elemental analysis (%) calcd for $C_{30}H_{24}N_6O_{18}P_6Zn_3Nd_2\cdot 4H_2O$: C 24.03, H 2.15, N 5.61; found: C 24.17, H 2.15, N 5.32; IR (KBr): $\tilde{\nu}$ = 3544(br), 1658(w), 1637(w), 1590(w), 1565(w), 1462(w), 1427(w), 1279(w), 1200(m), 1176(s), 1140(s), 1069(s), 1049(s), 1033(s), 1010(m), 979(s), 780(m), 735(m), 587(s), 564(m), 535(m) cm^{-1}.

X-ray crystallographic analysis: The intensity data for **1·Ln** (Ln = La, Ce, Pr, Nd), **2·Ln** (Ln = Pr, Nd, Sm, Eu, Gd, Tb, Dy, Ho), and **Nd_2Zn_3** were collected on a Bruker SMART APEX CCD diffractometer with graphite-monochromatized $Mo_{K\alpha}$ radiation (λ = 0.71073 Å) at room temperature. The data were integrated with the Siemens SAINT program,[40] and the intensities corrected for Lorentzian factor, polarization, air absorption, and absorption due to variation in the path length through the detector faceplate. Absorption corrections were applied. The structures were solved by direct methods and refined on F^2 by full-matrix least-squares techniques with SHELXTL.[41] All non-hydrogen atoms were located from the Fourier maps and refined anisotropically. All H atoms were refined isotropically with the isotropic vibration parameters related to the non-H atom to which they are bonded. Crystallographic and refinement details of **1·Ln**, **2·Ln**, and **Nd_2Zn_3** are listed in Tables 2 and 3. Selected bond lengths and angles for **1·Ln**, **2·Ln**, and **Nd_2Zn_3** are given in Tables 4 and 5.

CCDC-630558–CCDC-630570 contain the supplementary crystallographic data for this paper. These data can be obtained free of charge from the Cambridge Crystallographic Data Centre via www.ccdc.cam.ac.uk/data_request/cif.

Acknowledgements

The authors thank the National Natural Science Fund for Distinguished Young Scholars (No. 20325103), NSFC (Nos. 20433020, 20573050 and 20631030), and the specialized research fund for the doctoral program of the Ministry of Education of China (No. 0205116201) for financial support, and Dr. Y. Song and Mr. T.-W. Wang for magnetic measurements.

[1] C. Benelli, D. Gatteschi, *Chem. Rev.* **2002**, *102*, 2369–2387.
[2] R. E. P. Winpenny, *Chem. Soc. Rev.* **1998**, *27*, 447–452.
[3] a) S. Osa, T. Kido, N. Matsumoto, N. Re, A. Pochaba, J. Mrozinski, *J. Am. Chem. Soc.* **2004**, *126*, 420–421; b) J.-P. Costes, F. Dahan, W. Wernsdorfer, *Inorg. Chem.* **2006**. *45*, 5–7; c) F. Mori, T. Nyui, T. Ishida, T. Nogami, K.-Y. Choi, H. Nojiri, *J. Am. Chem. Soc.* **2006**, *128*, 1440–1441.
[4] J.-P. Costes, J. M. Clemente-Juan, F. Dahan, J. Milon, *Inorg. Chem.* **2004**, *43*, 8200–8202.
[5] A. Bencini, C. Benelli, A. Caneschi, R. L. Carlin, A. Dei, D. Gatteschi, *J. Am. Chem. Soc.* **1985**, *107*, 8128–8136.
[6] M. Andruh, I. Ramade, E. Codjovi, O. Guillou, O. Kahn, J. C. Trombe, *J. Am. Chem. Soc.* **1993**, *115*, 1822–1829.
[7] M. L. Kahn, C. Mathonière, O. Kahn, *Inorg. Chem.* **1999**, *38*, 3692–3697.
[8] A. J. Blake, R. O. Gould, C. M. Grant, P. E. Y. Milne, S. Parsons, R. E. P. Winpenny, *J. Chem. Soc. Dalton Trans.* **1997**, 485–495.
[9] a) J.-P. Costes, F. Dahan, A. Dupuis, *Inorg. Chem.* **2000**, *39*, 165–168; b) R. Gheorghe, P. Cucos, M. Andruh, J.-P. Costes, B. Donnadieu, S. Shova, *Chem. Eur. J.* **2006**, *12*, 187–203.
[10] Y.-F. Zhou, F.-L. Jiang, D.-Q. Yuan, B.-L. Wu, R.-H. Wang, Z.-Z. Lin, M.-C. Hong, *Angew. Chem.* **2004**, *116*, 5783–5786; *Angew. Chem. Int. Ed.* **2004**, *43*, 5665–5668.
[11] F. He, M.-L. Tong, X.-L. Yu, X.-M. Chen, *Inorg. Chem.* **2005**, *44*, 559–565.
[12] A.-Q. Wu, G.-H. Guo, C. Yang, F.-K. Zheng, X. Liu, G.-C. Guo, J.-S. Huang, Z.-C. Dong, Y. Takano, *Eur. J. Inorg. Chem.* **2005**, 1947–1954.
[13] H.-Z. Kou, Y.-B. Jiang, A.-L. Cui, *Cryst. Growth Des.* **2005**, *5*, 77–79.
[14] a) J.-P. Costes, F. Dahan, A. Dupuis, J.-P. Laurent, *Inorg. Chem.* **2000**, *39*, 169–173; b) J.-P. Costes, F. Dahan, A. Dupuis, *Inorg. Chem.* **2000**, *39*, 5994–6000.
[15] J. Pauloviè, F. Cimpoesu, M. Ferbinteanu, K. Hirao, *J. Am. Chem. Soc.* **2004**, *126*, 3321–3331.
[16] a) H. L. Ngo, W. Lin, *J. Am. Chem. Soc.* **2002**, *124*, 14298–14299; b) O. R. Evans, H. L. Ngo, W. Lin, *J. Am. Chem. Soc.* **2001**, *123*, 10395–10396; c) K. L. Nash, R. D. Rogers, J. Ferraro, J. Zhang, *Inorg. Chim. Acta* **1998**, *269*, 211–223; d) F. Serpaggi, G. Férey, *J. Mater. Chem.* **1998**, *8*, 2749–2755; e) F. Serpaggi, G. Férey, *Inorg. Chem.* **1999**, *38*, 4741–4744; f) C. Serre, N. Stock, T. Bein, G. Férey, *Inorg. Chem.* **2004**, *43*, 3159–3163; g) J.-L. Song, J.-G. Mao, *Chem. Eur. J.* **2005**, *11*, 1417–1424; h) J.-L. Song, C. Lei, J.-G. Mao, *Inorg.*

Chem. **2004**, *43*, 5630–5634; i) R.-C. Wang, Y. Zhang, H. Hu, R. R. Frausto, A. Clearfield, *Chem. Mater.* **1992**, *4*, 864–871; j) E. Galdecka, Z. Galdecki, P. Gawryszewska, J. Legendziewicz, *New J. Chem.* **2000**, *24*, 387–391; k) D.-K. Cao, Y.-Z. Li, Y. Song, L.-M. Zheng, *Inorg. Chem.* **2005**, *44*, 3599–3604; l) J. A. Groves, P. A. Wright, P. Lightfoot, *Inorg. Chem.* **2005**, *44*, 1736–1739.

[17] Y.-S. Ma, Y. Song, W.-X. Du, Y.-Z. Li, L.-M. Zheng, *Dalton Trans.* **2006**, 3228–3235.

[18] G. E. Pringle, *Acta Crystallogr. Sect. B* **1972**, *28*, 2326–2328.

[19] A. L. Spek, Platon: A Multi-purpose Crystallographic Tool, Utrecht University, Utrecht, The Netherlands, **2001**.

[20] a) L. Carlucci, G. Ciani, D. M. Proserpio, A. Sironi, *J. Am. Chem. Soc.* **1995**, *117*, 12861–12862; b) S. Decurtins, H. W. Schmalle, P. Schneuwly, H. R. Oswald, *Inorg. Chem.* **1993**, *32*, 1888–1892; c) L. Carlucci, G. Ciani, D. M. Proserpio, A. Sironi, *Chem. Commun.* **1996**, 1393–1394; d) O. M. Yaghi, C. E. Davis, G.-M. Li, H.-L. Li, *J. Am. Chem. Soc.* **1997**, *119*, 2861–2868; e) A. B. Mallik, S. Lee, E. B. Lobkovsky, *Cryst. Growth Des.* **2005**, *5*, 609–616.

[21] D. H. Templeton, C. H. Dauben, *J. Am. Chem. Soc.* **1954**, *76*, 5237–5239.

[22] A. D. Becke, *J. Chem. Phys.* **1993**, *98*, 5648–5654.

[23] C. Lee, W. Yang, R. G. Parr, *Phys. Rev. B* **1988**, *37*, 785–789.

[24] Gaussian 98, Revision A.11.3, M. J. Frisch, G. W. Trucks, H. B. Schlegel, G. E. Scuseria, M. A. Robb, J. R. Cheeseman, J. A. Montgomery, T. Jr.Vreven, K. N. Kudin, J. C. Burant, J. M. Millam, S. S. Iyengar, J. Tomasi, V. Barone, B. Mennucci, M. Cossi, G. Scalmani, N. Rega, G. A. Petersson, H. Nakatsuji, M. Hada, M. Ehara, K. Toyota, R. Fukuda, J. Hasegawa, M. Ishida, T. Nakajima, Y. Honda, O. Kitao, H. Nakai, M. Klene, X. Li, J. E. Knox, H. P. Hratchian, J. B. Cross, C. Adamo, J. Jaramillo, R. Gomperts, R. E. Stratmann, O. Yazyev, A. J. Austin, R. Cammi, C. Pomelli, J. W. Ochterski, P. Y. Ayala, K. Morokuma, G. A. Voth, P. Salvador, J. J. Dannenberg, V. G. Zakrzewski, S. Dapprich, A. D. Daniels, M. C. Strain, O. Farkas, D. K. Malick, A. D. Rabuck, K. Raghavachari, J. B. Foresman, J. V. Ortiz, Q. Cui, A. G. Baboul, S. Clifford, J. Cioslowski, B. B. Stefanov, G. Liu, A. Liashenko, P. Piskorz, I. Komaromi, R. L. Martin, D. J. Fox, T. Keith, M. A. Al-Laham, C. Y. Peng, A. Nanayakkara, M. Challacombe, P. M. W. Gill, B. Johnson, W. Chen, M. W. Wong, C. Gonzalez, J. A. Pople, Gaussian, Inc., Pittsburgh, PA, **2002**.

[25] M. Dolg, H. Stoll, A. Savin, H. Preuss, *Theor. Chim. Acta* **1989**, *75*, 173–194.

[26] P. J. Hay, W. R. Wadt, *J. Chem. Phys.* **1985**, *82*, 299–310.

[27] L. E. Chirlian, M. M. Francl, *J. Comput. Chem.* **1987**, *8*, 894–905.

[28] C. M. Breneman, K. B. Wiberg, *J. Comput. Chem.* **1990**, *11*, 361–373.

[29] M. M. Francl, C. Carey, L. E. Chirlian, D. M. Gange, *J. Comput. Chem.* **1996**, *17*, 367–383.

[30] H. J. C. Berendsen, J. P. M. Postma, W. F. van Gunsteren, J. Hermans, "Interaction Models for Water in Relation to Protein Hydration" in *Intermolecular Forces* (Ed.: B. Pullman), D. Reidel, Amsterdam, **1981**, pp. 331–342.

[31] N. Karasawa, W. A. Goddard, *J. Phys. Chem.* **1989**, *93*, 7320–7327.

[32] A. K. Rappé, C. J. Casewit, K. S. Colwell, W. A. Goddard, W. M. Skiff, *J. Am. Chem. Soc.*, **1992**, *114*, 10024–10035.

[33] C. J. Casewit, K. S. Colwell, A. K. Rappé, *J. Am. Chem. Soc.* **1992**, *114*, 10035–10046.

[34] C. J. Casewit, K. S. Colwell, A. K. Rappé, *J. Am. Chem. Soc.* **1992**, *114*, 10046–10053.

[35] A. K. Rappé, K. S. Colwell, C. J. Casewit, *Inorg. Chem.* **1993**, *32*, 3438–3450.

[36] Cerius2, Version 3.5, Molecular Simulation Inc., San Diego, CA, **1997**.

[37] a) D.-K. Cao, Y.-J. Liu, Y. Song, L.-M. Zheng, *New J. Chem.* **2005**, *29*, 721–725; b) Y. Wang, S.-S. Bao, W. Xu, J. Chen, S. Gao, L.-M. Zheng, *J. Solid State Chem.* **2004**, *177*, 1297–1300.

[38] J. S. Loran, R. A. Naylor, A. Williams, *J. Chem. Soc. Perkin Trans. 2* **1976**, *12*, 1444–1447.

[39] O. Kahn, *Molecular Magnetism*, VCH Publishers, New York, 1 **993**.

[40] SAINT, Program for Data Extraction and Reduction, Siemens Analytical X-ray Instruments, Madison, WI, **1994–1996**.

[41] SHELXTL (version 5.0), Reference Manual, Siemens Industrial Automation, Analytical Instruments, Madison, WI, **1995**.

Received: December 13, 2006
Published online: March 20, 2007

